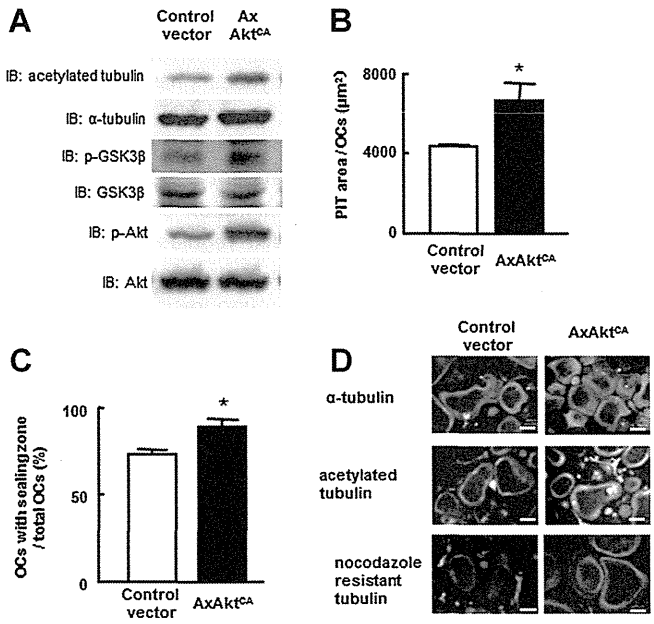

Fig. 2. Effect of forced activation of Akt on microtubule stabilization and bone-resorbing activity in osteoclasts. (*A*) Western blotting showing the effects of adenovirus vector-mediated expression of constitutively active Akt1 on the expression level of acetylated tubulin, phospho-GSK3β, and phospho-Akt. The blots were reprobed with an anti-α-tubulin antibody, anti-GSK3β antibody, and anti-Akt antibody. Resorption pit area per cell (*B*) and the proportion of cells with the sealing zone (*C*) in osteoclasts infected with the control vector or AxAkt^{CA}. $^{*}p < 0.01$ versus control. (*D*) Osteoclasts infected with control vector or AxAkt^{CA} were fixed and visualized under fluorescence microscopy after the staining of α-tubulin (top panel) and acetylated-tubulin (middle panel). After treatment with 1 μM nocodazole for 30 minutes, osteoclasts were fixed and stained with an anti-α-tubulin antibody (bottom panel). Scale bars = 50 μm.

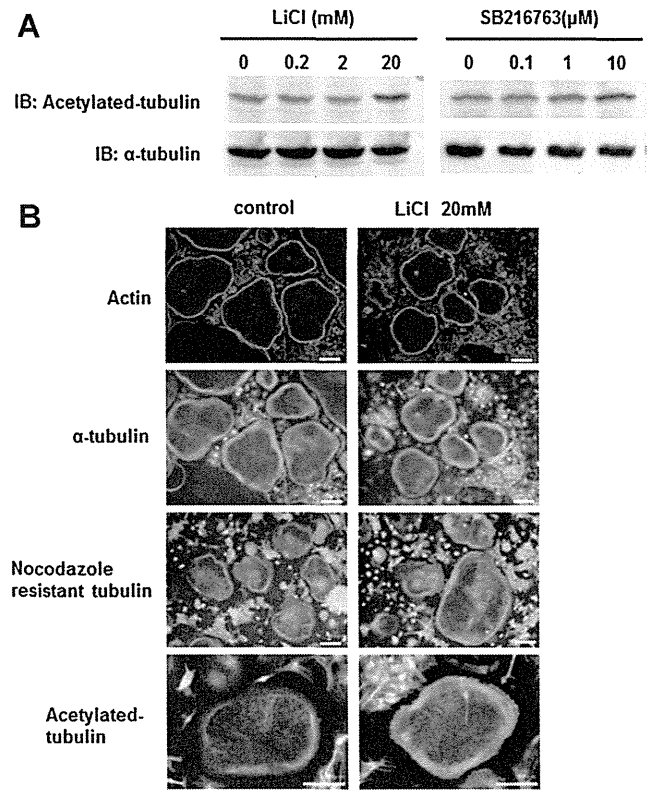

Fig. 3. Effect of GSK-3β inhibitors on microtubule stabilization in osteoclasts. (*A*) Western blotting showing the dose-dependent effect of LiCl and SB216763 on the expression level of acetylated-tubulin in osteoclasts. The blots were reprobed with an anti-α-tubulin antibody. (*B*) Osteoclasts cultured with or without 20 mM LiCl were fixed and visualized under fluorescence microscopy after staining for actin (top panel), α-tubulin (second top panel), and acetylated tubulin (bottom panel). Osteoclasts incubated with or without 20 mM LiCl were treated with 1 μM nocodazole for 30 minutes and then fixed and stained with an anti-α-tubulin antibody (second panel from bottom). Scale bars = 100 μm.

osteoclasts, whereas the osteoclasts infected with AxAkt^{CA} contained a nocodazole-resistant pool of stable microtubules (Fig. 2*D*).

GSK3β inhibition affects the stabilization of microtubules

To confirm that the increased acetylated tubulin formation was regulated through the Akt/GSK-3β axis, we assessed the effect of LiCl and SB216763, which are specific inhibitors of GSK-3β. The osteoclasts were cultured for 5 hours in the presence of the indicated concentrations of LiCl or SB216763. LiCl and SB216763 dose-dependently increased the expression of the acetylated tubulin (Fig. 3*A*). Immunofluorescence analysis showed that the treatment with LiCl did not affect the structure of actin or tubulin, but rather induced the accumulation of the acetylated tubulin throughout the entire cytoplasm and increased the nocodazole-resistant pool of stable microtubules (Fig. 3*B*).

Akt regulates microtubule formation through GSK-3β

We next examined the involvement of Akt/GSK-3β in the dynamic formation of tubulin. The disrupted tubulin structure that had lost its circular pattern at the cell periphery as the result of nocodazole treatment was restored within 1 or 2 hours after the removal of nocodazole (Fig. 4*A*). Such recovery was not observed in osteoclasts treated with the Akt inhibitor and was promoted in the cells treated with LiCl. In accordance with the formation of the microtubules, the nuclei gathered in the center of the cell after nocodazole treatment were rearranged in the cell periphery in the control osteoclasts. This nuclear translocation was quantified by measuring the proportion of the nuclei placed at the cell periphery among all of the nuclei (peripheral nuclear translocation ratio, PNT ratio). The PNT ratio was significantly reduced by nocodazole treatment (67% ± 20% versus 9% ± 7%, $p < 0.01$), and recovered to the basal level within 60 minutes in the control osteoclasts and 30 minutes in the cells treated with LiCl. In contrast, the decreased PNT ratio was not fully recovered even 120 minutes after the removal of nocodazole in osteoclasts cultured in the presence of the Akt inhibitor (Fig. 4*B*). These results suggested that Akt correlates with the formation of microtubules and the accompanying nuclear translocation, which is mediated by GSK-3β.

The binding of MAPs with tubulin is regulated by Akt

Nuclear migration is known to be mediated by the activity of dynein/dynactin at the cell cortex.[19] The dynactin complex is

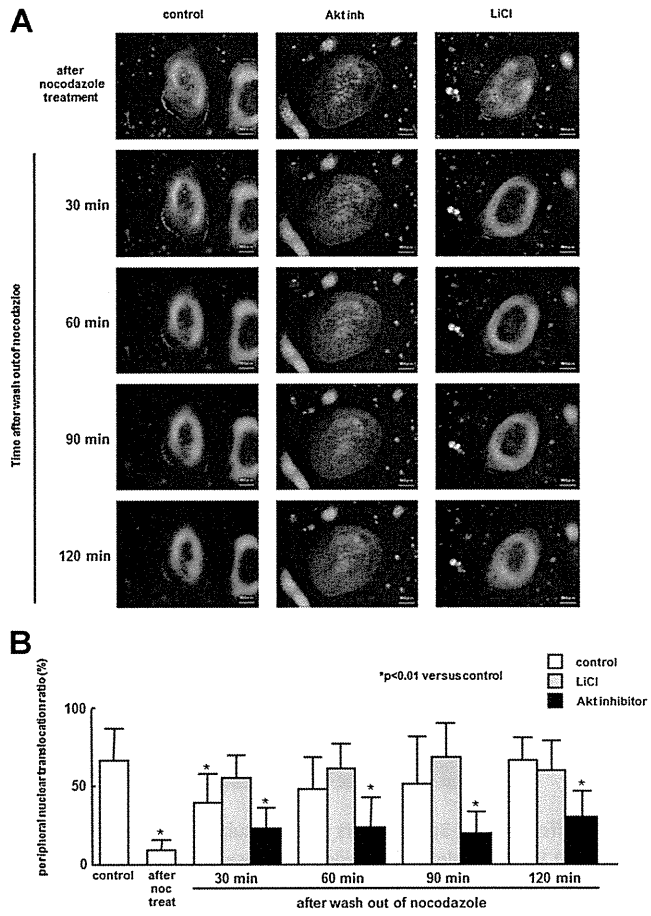

Fig. 4. Dynamics of cytoskeletal reorganization after nocodazole treatment in the presence of the Akt inhibitor or LiCl. (*A*) Osteoclasts cultured on glass coverslips were infected with AxTb-YFP and stained with Hoechst 33258. After nocodazole treatment, osteoclasts were incubated with α-MEM (control) or α-MEM containing 1 μM (Akt inhibitor IV or α-MEM containing 20 mM LiCl (LiCl) in a thermostat bearing chamber for microscopic analysis, and were examined under fluorescence microscopy for 120 minutes. Stills from the time-lapse videos are shown. (*B*) The proportion of the nuclei involved in the circular division of microtubules at the cell periphery per the overall number of nuclei in the cells (peripheral nuclear translocation [PNT] ratio) was calculated in 100 osteoclasts in each group at the indicated time point. The experiments were repeated three times, and the results are expressed as the mean ± SD of the PNT ratio in a total of 300 osteoclasts. $^{*}p < 0.01$ versus control.

able to bind to both microtubules and dynein, and activates dynein's minus-end–directed motor activity. Many +TIPs, including dynactin, have important roles in anchoring and stabilizing microtubules. At the cell cortex, where microtubules are captured, dynein's minus-end–directed motor activity is converted to a force that pulls nuclei toward the cortex. Taken together, these findings indicate that the anchoring of microtubules to the cytoplasmic membrane is regulated by Akt in osteoclasts.

We therefore compared the binding of several representative MAPs to the Triton cytoskeleton between osteoclasts infected with control adenovirus vector or AxAkt^{CA}. Among the MAPs examined, the amount of EB1, APC, and p150Glued anchored to the Triton cytoskeleton was increased in osteoclasts infected with AxAkt^{CA} compared to control osteoclasts (Fig. 5*A*). p150Glued, a major component of dynactin, has sites that bind to EB1 and dynein.[20] Mammalian EB1 and APC directly bind to each other and cooperate in the regulation of microtubule dynamics and microtubule-dependent processes under diverse conditions, including cell migration and mitosis.[21,22] We therefore examined whether Akt regulates the EB1-APC complex formation in osteoclasts. In control vector or AxAkt^{CA}-infected osteoclasts, APC was coimmunoprecipitated with EB1 (Fig. 5*B*). An association between EB1 and APC was observed in both the control and AxAkt^{CA}-infected osteoclasts, and the level of APC was substantially increased by AxAkt^{CA} infection (Fig. 5*B*).

Colocalization of EB1 and APC is lost in Akt1-deficient and Akt2-deficient osteoclasts

To further confirm the role of Akt in regulating MAPs, we generated osteoclast-specific Akt1 and Akt2 conditional knockout mice by crossing Akt1$^{fl/fl}$, Akt2$^{fl/fl}$, and cathepsin K-Cre knock-in mice.[14] The cathepsin K-Cre$^{+/-}$Akt1$^{fl/fl}$Akt2$^{fl/fl}$ mice (referred to herein as DKO mice) were born alive at the predicted Mendelian frequencies. Akt1 and Akt2 were markedly reduced in the osteoclasts from the DKO mice, whereas their expression in osteoblasts (Fig. 6*A*) and other tissues (data not shown) in DKO mice was comparable to that found in normal Akt1$^{fl/fl}$Akt2$^{fl/fl}$ littermates (referred to herein as DF mice representing double flox) (Fig. 6*A*). Osteoclasts were generated from bone marrow cells obtained from DKO or DF mice using receptor activator of NF-κB ligand (RANKL) and macrophage colony-stimulating factor (M-CSF). There was no apparent difference in RANKL-induced and M-CSF–induced osteoclast development or osteoclast-related gene expression between DKO and DF bone marrow cells (data not shown). Immunoprecipitation of EB1 from both DKO and DF osteoclasts showed that the association between EB1 and APC was substantially reduced by the deletion of Akt1 and Akt2 (Fig. 6*B*). Immunofluorescence analysis demonstrated that in the DF osteoclasts intense labeling of APC was detected in and around the nuclei and at the cell periphery, and APC colocalized well with EB1 except in the nuclei. In contrast, APC staining in DKO osteoclasts was detected potently in and around the nuclei and faintly at the cell periphery, and colocalized well with EB1 only around the nuclei (Fig. 6*C*). These results suggest that Akt has a role in regulating APC-EB1 complex formation in osteoclasts. We then compared the pit-forming activity and the sealing zone formation in the DF and DKO osteoclasts. The DKO osteoclasts exhibited a reduced bone-resorbing activity and sealing zone formation compared to the DF osteoclasts, which effect was recovered by the addition of LiCl (Fig. 6*D–G*).

Osteoclast-specific Akt1-deficient and Akt2-deficient mice shows increased bone mass due to impaired absorption of osteoclasts

Although Akt DKO mice grew normally with no apparent morphological abnormalities, 12-week-old Akt DKO mice exhibited increased bone mass compared to their littermate DF mice on radiographic (Fig. 7*A*) and histological analyses (Fig. 7*D*). μCT analysis revealed a significant increase in bone

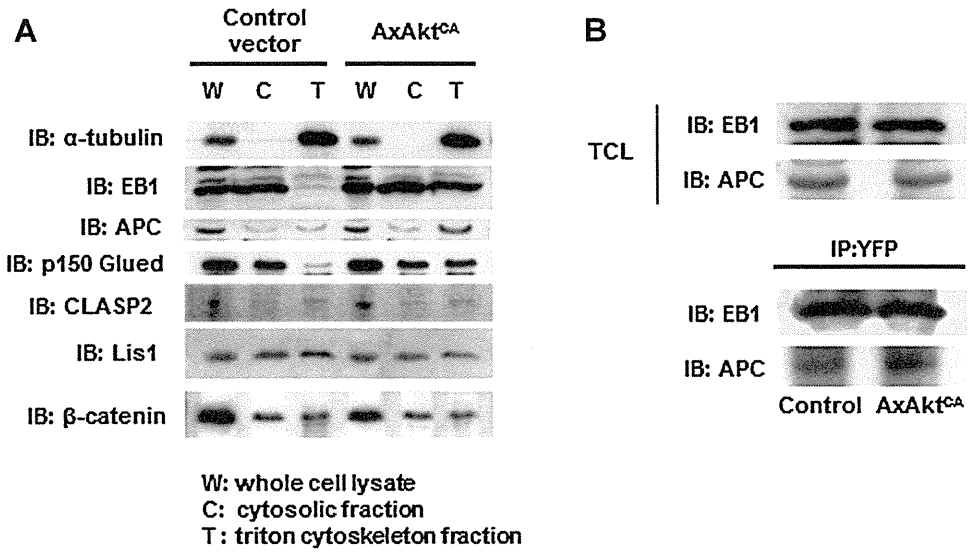

Fig. 5. The binding of MAPs is regulated by Akt. (*A*) Whole-cell lysate (W), the cytosolic fraction (C), and triton cytoskeleton fraction (T) obtained from osteoclasts infected with control vector or AxAkt^{CA} were immunoblotted with an anti-EB1 antibody, anti-APC antibody, anti-p150 Glued antibody, anti-CLASP2 antibody, anti-Lis1 antibody, and anti-β-catenin antibody; α-tubulin is shown as a control. (*B*) Osteoclasts were infected with AxEB1-YFP. Cell lysates were immunoprecipitated with an anti-YFP antibody and analyzed by Western blot with an anti-EB1 antibody and anti-APC antibody. IP = immunoprecipitates; IB = immunoblotting.

volume per tissue volume and a significant decrease in trabecular separation compared with normal Akt DF littermates (Fig. 7*B*, *C*). There was no significant difference in trabecular thickness or trabecular number between the DKO mice and their normal littermates (Fig. 7*C*). Histomorphometric analysis of 12-week-old Akt DKO mice revealed a significant increase in the bone volume of the primary spongiosa (Fig. 7*D*). The number of osteoclasts per bone perimeter measurement and the extent of the eroded surface were decreased in DKO mice. A noteworthy finding in the DKO mice was the increase in the number of rounded osteoclasts detached from the bone surface (Fig. 7*E*), and the ratio of detached osteoclasts per total osteoclasts was significantly higher in the DKO mice compared with the DF mice (27.9% ± 4.6% versus 9.1% ± 2.3%, $p < 0.01$) (Fig. 7*F,G*). These mice also displayed an apparent, although not significant, decrease in the mineral apposition rate and displayed a significant decrease in the bone formation rate, indicating a low turnover of the bone metabolism. These findings suggest that the increased bone mass observed in the Akt DKO mice was caused by a decrease in the bone-resorbing activity of mature osteoclasts, rather than by increased bone formation per se.

Discussion

Previous studies have revealed various roles of Akt in osteoclasts. M-CSF and RANKL promote osteoclast survival in part by activating the Akt pathway.[23,24] Sugatani and Hruska[25] reported in a study using small interfering RNA (siRNA) that Akt1/Akt2 plays an essential role in the differentiation, but not in the survival of osteoclasts. Several other studies demonstrated the role of Akt in the survival of osteoclasts.[23,24] We previously reported that Akt regulates bone-resorbing activity through its organizing effect on the formation of sealing zones.[26] In this study, we have presented in vitro and in vivo evidence that Akt positively regulates osteoclast activity by controlling microtubule stability.

There is accumulating evidence that the actin organization in osteoclasts is regulated by microtubules.[7,8] In particular, acetylated tubulin is reported to be important for changes in the podosome structure during osteoclast maturation.[2,9] Hazama and colleagues[10] reported that deacetylation of acetylated tubulin is essential for the secretion of the lytic granules needed for bone resorption. We showed by immunofluorescence staining that an Akt inhibitor disturbed podosome belt formation in mature osteoclasts with a dysregulation of acetylated tubulin (Fig. 1*E*). The acetylated tubulin expression level was increased in osteoclasts expressing Akt^{CA}, suggesting that Akt positively regulates microtubule stability.

At the plus-end, microtubules continuously switch between assembly and disassembly, a phenomenon called "dynamic instability." MAPs bind to the microtubules to regulate their stability, and some MAPs have a role in stabilizing microtubules and mediating their interaction with the cell cortex. The interaction between these MAPs and tubulin is lost upon phosphorylation by GSK-3β, which is negatively regulated by Akt.[27] An Akt inhibitor blocked the peripheral translocation of the nuclei and microtubules to the cell periphery, whereas LiCl stimulated it, suggesting that these phenomena are positively controlled by the Akt/GSK-3β axis.

Nuclear migration is an important event associated with many cellular events such as migration and division, in which dynein, a minus-end–directed motor, is known to be involved.[19,28,29] The dynein anchored to the cell cortex has been proposed to reel in the microtubules and the nuclei attached to these microtubules.[19] The observation that nuclear migration is promoted

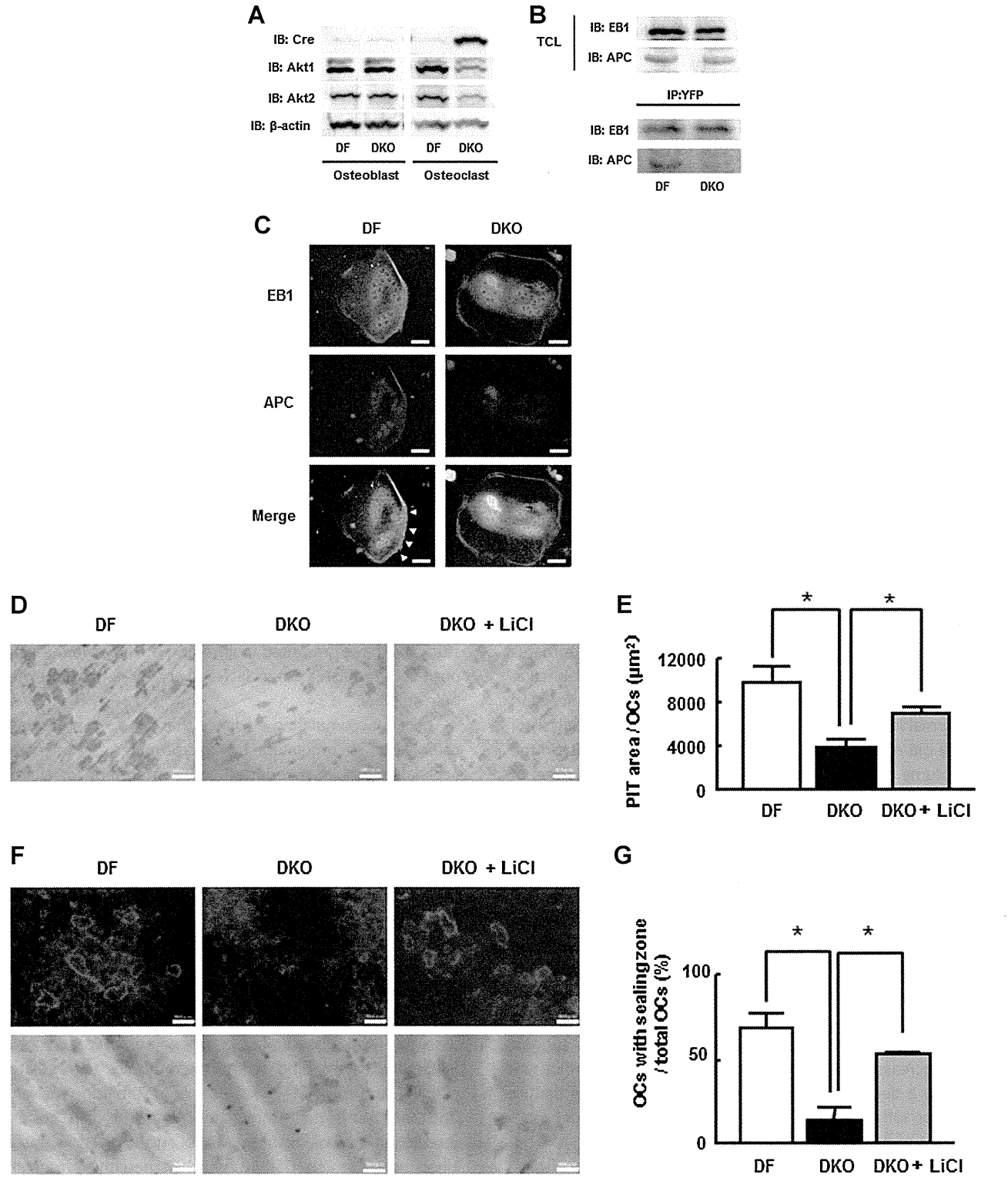

Fig. 6. Reduced bone-resorbing activity and its rescue by LiCl in Akt1 and Akt2 deficient osteoclasts. (*A*) Western blotting of Cre recombinase, Akt1, and Akt2 in osteoblasts and osteoclasts derived from osteoclast-specific Akt1 and Akt2 double-knockout mice (DKO) and their normal littermates (DF) using β-actin as an internal control. (*B*) Osteoclasts generated from bone marrow cells of the DKO and DF mice were infected with AxEB1-YFP. Cell lysates were immunoprecipitated with an anti-YFP antibody and analyzed by Western blot with an anti-EB1 antibody and anti-APC antibody. IP = immunoprecipitates; IB = immunoblotting. (*C*) DF and DKO osteoclasts were fixed and stained to visualize EB1 and APC. The arrowheads indicate an example of the colocalization of EB1 and APC at the cell periphery, which appears in yellow. Scale bars = 50 μm. (*D*) The resorption pits generated by DF and DKO osteoclasts and the effect of LiCl on the bone-resorbing activity of DKO osteoclasts. Scale bars = 100 μm. (*E*) Resorption pit area per osteoclast. $^{*}p < 0.01$. (*F*) Sealing zone formation on dentin slices in the DF and DKO osteoclasts and the effect of LiCl on the sealing zone formation in DKO osteoclasts. Scale bars = 50 μm. (*G*) Proportion of osteoclasts with sealing zones. $^{*}p < 0.01$.

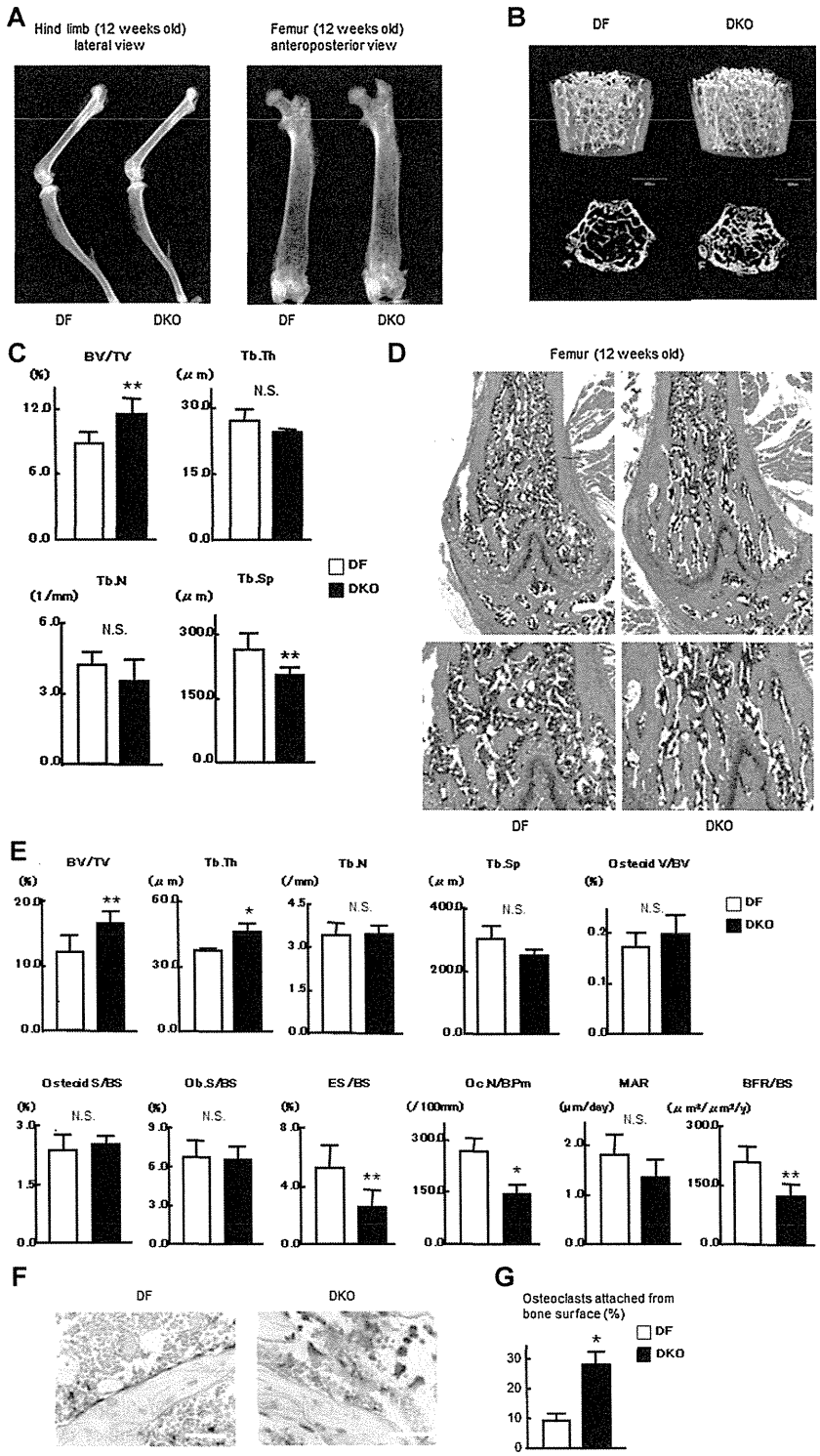

Fig. 7. Skeletal analysis of Akt1 and Akt2 *DKO* mice. (*A*) Radiographic analysis of Akt1 and Akt2 double-conditional knockout mice and their normal littermates at 12 weeks of age. (*B*) μCT of the distal femur of the DKO mice and their normal littermates at 12 weeks of age. (*C*) Quantification of the μCT data. Data are expressed as the mean ± SD from five mice of each genotype. Trabecular bone volume fraction (BV/TV), trabecular bone thickness (Tb.Th), trabecular bone number (Tb.N), and trabecular separation (Tb.Sp) in the DF and DKO mice. $^{**}p < 0.05$ versus DF mice. (*D*) Histological sections of the distal femur from DF and DKO mice at 12 weeks. (*E*) Histomorphometric analysis: the parameters were measured in the proximal tibia of the DF and DKO mice. Data are expressed as the mean ± SD from five mice of each genotype. BV/TV = trabecular bone volume expressed as a percentage of the tibial tissue volume; Tb.Th = trabecular bone thickness; Tb.N = trabecular bone number per mm; Tb.Sp = average space between neighboring trabecular bones; Osteoid V/BV = osteoid volume per bone volume; Osteoid S/BS = percentage of bone surface covered by osteoid; Ob.S/BS = percentage of the bone surface covered by cuboidal osteoblast; ES/BS = percentage of eroded surface; Oc.N/B.Pm = number of mature OCs per 100 mm of bone perimeter; MAR = mineral apposition rate, the rate (in μm/d) at which new bone is being added to cancellous surfaces; BFR = estimate of the cancellous bone volume that is being replaced annually. $^{**}p < 0.05$ versus DF mice. (*F*) TRAP staining of the proximal tibia from the DF and DKO mice. Scale bars = 50 μm. (*G*) Proportion of osteoclasts attached (from) to the bone surface. $^{*}p < 0.01$ versus DF mice.

by the activation of Akt or inhibition of GSK-3β raises the possibility that the proteins involved in the anchoring of dynein to the cell cortex are regulated by the Akt/GSK-3β pathway. Evidence has been accumulating that dynamics and organization of the microtubules are regulated by PI3K and its downstream kinases Akt and GSK-3β. For example, centrosome separation and mitotic spindle orientation in *Drosophila melanogaster* are facilitated by the stabilization that takes place between the microtubules and cortex, which is mediated by Akt and Zeste-white 3 (Zw3; the *D. melanogaster* homologue of GSK-3).[30] In migrating fibroblasts, microtubule stabilization is regulated at the leading edge, which is regulated by the PI3K/Akt pathway.[31] To date, several classes of proteins have been shown to be associated with the microtubule plus-ends and to interact with each other.[32] Our study revealed that the forced activation of Akt increased the association of p150Glued, EB1, and APC with the triton-insoluble cytoskeleton fraction. EB1 associates with the newly growing microtubule plus-end, coupled with a rapid dissociation from the older part.[33] EB1 is considered to play an essential role in microtubule dynamics by regulating the connection between microtubules and various microtubule trapping proteins on the cell cortex.[20] APC is classified as a tumor suppressor gene, and its mutations are known to cause familial adenomatous polyposis.[34] APC can stabilize microtubules directly by interacting with microtubules with its microtubule-binding region located between amino acids 2219 and 2580,[35,36] or indirectly by interacting with EB1.[21] The interaction between APC and EB1 is reported to be important for the formation of stable microtubules in migrating fibroblasts[37] and the carrying out of mitosis.[38] Phosphorylation by GSK-3β decreases the ability of APC to bind to microtubules, which results in decreased microtubule stability.[39] Akt facilitates a stable interaction between the cell cortex and microtubules by phosphorylating GSK-3β and decreasing its activity.[27] p150Glued, one of the proteins that accumulate in the Triton-insoluble cytoskeletal fraction in osteoclasts infected with $Ax Akt^{CA}$, is a major component of the dynactin complex which mediates dynein-driven activity. Because dynein directly associates with EB1,[40] it is speculated that Akt promotes the motility of microtubules and nuclei by connecting dynein to the cell cortex through the APC-EB1 complex. In fact, immunofluorescence staining of DKO osteoclasts revealed a decreased colocalization of APC and EB1 at the cell periphery. The decreased bone-resorbing activity and inhibition of sealing zone formation in Akt DKO osteoclasts were both recovered by an inhibition of GSK-3β activity with LiCl.

Mice lacking the Akt1 gene are viable but their size is small compared to wild-type littermates.[41] Kawamura and colleagues[42] revealed that conventional Akt1 knockout mice exhibit low-turnover osteoporosis as a result of the impeded differentiation and survival of osteoblasts and osteoclasts. They speculated that the impaired differentiation of osteoclasts in Akt1 knockout mice is due to a reduced expression of RANKL in osteoblasts and the direct effect of this on osteoclasts. Akt2 knockout mice exhibit insulin resistance, with elevated blood glucose, mild growth deficiency, and an age-dependent loss of adipose tissue.[43,44] Mice lacking both the Akt1 gene and the Akt2 gene die shortly after birth, exhibiting severe growth deficiency, muscle atrophy, and impeded adipogenesis.[45] To elucidate the physiological role of Akt in osteoclasts, we generated osteoclast-specific Akt1 and Akt2 double-knockout mice. We found that the mice exhibited mild osteosclerosis as a result of the decreased bone-resorbing activity of osteoclasts, which is consistent with the in vitro results using osteoclasts generated from DKO mouse bone marrow cells. The lack of Akt1/2 did not completely inhibit bone resorption either in vivo or in vitro. This may be because the deletion efficiency of Akt1 and Akt2 in DKO was not complete enough, as shown in Fig. 6*A*, or there may be other molecule(s) that substitute the function of Akt1/2.

In summary, our results provide both in vivo and in vitro evidence that the signaling pathways regulated by the Akt/GSK-3β axis play an essential role in normal osteoclast function by regulating cytoskeletal organization. Further investigation of these pathways in osteoclasts will provide further insights into the molecular mechanisms regulating cytoskeletal organization and function.

Disclosures

All authors state that they have no conflicts of interest.

Acknowledgments

This work was supported by Grants-in-Aid from the Ministry of Education, Culture, Sports, Science, and Technology of Japan and Health Science research grants from the Ministry of Health, Labor, and Welfare of Japan (to ST and YK). We thank Reiko Yamaguchi and Hajime Kawahara (Department of Orthopaedic Surgery, The University of Tokyo), who provided expert technical assistance. Pacific Edit reviewed the manuscript prior to submission.

Authors' roles: Study design and conception: TM, ST. Study conduct and data collection: TM, YN, JH, NT, TY. Data analysis: TM, YN, YK, ST. Data interpretation: TM, YK, KU, TK, KN, ST. Drafting manuscript: TM, ST. Revising manuscript content: All authors. Approving final version of manuscript: All authors. TM and ST take responsibility for the integrity of the data analysis.

References

1. Collin O, Tracqui P, Stephanou A, Usson Y, Clement-Lacroix J, Planus E. Spatiotemporal dynamics of actin-rich adhesion microdomains: influence of substrate flexibility. J Cell Sci. 2006;119(Pt 9):1914–25.
2. Destaing O, Saltel F, Geminard JC, Jurdic P, Bard F. Podosomes display actin turnover and dynamic self-organization in osteoclasts expressing actin-green fluorescent protein. Mol Biol Cell. 2003;14(2):407–16.
3. Mulari MT, Zhao H, Lakkakorpi PT, Vaananen HK. Osteoclast ruffled border has distinct subdomains for secretion and degraded matrix uptake. Traffic. 2003;4(2):113–25.
4. Luxenburg C, Geblinger D, Klein E, Anderson K, Hanein D, Geiger B, Addadi L. The architecture of the adhesive apparatus of cultured osteoclasts: from podosome formation to sealing zone assembly. PLoS One. 2007;2(1):e179.
5. Holy TE, Leibler S. Dynamic instability of microtubules as an efficient way to search in space. Proc Natl Acad Sci U S A. 1994;91(12):5682–5.

6. Mulari MT, Patrikainen L, Kaisto T, Metsikko K, Salo JJ, Vaananen HK. The architecture of microtubular network and Golgi orientation in osteoclasts—major differences between avian and mammalian species. Exp Cell Res. 2003;285(2):221–35.
7. Jurdic P, Saltel F, Chabadel A, Destaing O. Podosome and sealing zone: specificity of the osteoclast model. Eur J Cell Biol. 2006; 85(3–4):195–202.
8. Okumura S, Mizoguchi T, Sato N, Yamaki M, Kobayashi Y, Yamauchi H, Ozawa H, Udagawa N, Takahashi N. Coordination of microtubules and the actin cytoskeleton is important in osteoclast function, but calcitonin disrupts sealing zones without affecting microtubule networks. Bone. 2006;39(4):684–93.
9. Destaing O, Saltel F, Gilquin B, Chabadel A, Khochbin S, Ory S, Jurdic P. A novel Rho-mDia2-HDAC6 pathway controls podosome patterning through microtubule acetylation in osteoclasts. J Cell Sci. 2005;118(Pt 13):2901–11.
10. Hazama R, Qu X, Yokoyama K, Tanaka C, Kinoshita E, He J, Takahashi S, Tohyama K, Yamamura H, Tohyama Y. ATP-induced osteoclast function: the formation of sealing-zone like structure and the secretion of lytic granules via microtubule-deacetylation under the control of Syk. Genes Cells. 2009;14(7):871–84.
11. Hanada M, Feng J, Hemmings BA. Structure, regulation and function of PKB/AKT—a major therapeutic target. Biochim Biophys Acta. 2004;1697(1–2):3–16.
12. Wan M, Easton RM, Gleason CE, Monks BR, Ueki K, Kahn CR, Birnbaum MJ. Loss of Akt1 in mice increases energy expenditure and protects against diet-induced obesity. Mol Cell Biol. 2012;32(1):96–106.
13. Leavens KF, Easton RM, Shulman GI, Previs SF, Birnbaum MJ. Akt2 is required for hepatic lipid accumulation in models of insulin resistance. Cell Metab. 2009;10(5):405–18.
14. Nakamura T, Imai Y, Matsumoto T, Sato S, Takeuchi K, Igarashi K, Harada Y, Azuma Y, Krust A, Yamamoto Y, Nishina H, Takeda S, Takayanagi H, Metzger D, Kanno J, Takaoka K, Martin TJ, Chambon P, Kato S. Estrogen prevents bone loss via estrogen receptor alpha and induction of Fas ligand in osteoclasts. Cell. 2007;130(5):811–23.
15. Miyazaki T, Katagiri H, Kanegae Y, Takayanagi H, Sawada Y, Yamamoto A, Pando MP, Asano T, Verma IM, Oda H, Nakamura K, Tanaka S. Reciprocal role of ERK and NF-kappaB pathways in survival and activation of osteoclasts. J Cell Biol. 2000;148(2):333–42.
16. Black MM, Aletta JM, Greene LA. Regulation of microtubule composition and stability during nerve growth factor-promoted neurite outgrowth. J Cell Biol. 1986;103(2):545–57.
17. Tanaka S, Takahashi T, Takayanagi H, Miyazaki T, Oda H, Nakamura K, Hirai H, Kurokawa T. Modulation of osteoclast function by adenovirus vector-induced epidermal growth factor receptor. J Bone Miner Res. 1998;13(11):1714–20.
18. Turksen K, Kanehisa J, Opas M, Heersche JN, Aubin JE. Adhesion patterns and cytoskeleton of rabbit osteoclasts on bone slices and glass. J Bone Miner Res. 1988;3(4):389–400.
19. Bloom K. Nuclear migration: cortical anchors for cytoplasmic dynein. Curr Biol. 2001;11(8):R326–9.
20. Akhmanova A, Hoogenraad CC. Microtubule plus-end-tracking proteins: mechanisms and functions. Curr Opin Cell Biol. 2005;17(1): 47–54.
21. Su LK, Burrell M, Hill DE, Gyuris J, Brent R, Wiltshire R, Trent J, Vogelstein B, Kinzler KW. APC binds to the novel protein EB1. Cancer Res. 1995;55(14):2972–7.
22. Morrison EE. The APC-EB1 interaction. Adv Exp Med Biol. 2009; 656:41–50.
23. Wong BR, Besser D, Kim N, Arron JR, Vologodskaia M, Hanafusa H, Choi Y. TRANCE, a TNF family member, activates Akt/PKB through a signaling complex involving TRAF6 and c-Src. Mol Cell. 1999;4(6): 1041–9.
24. Gingery A, Bradley E, Shaw A, Oursler MJ. Phosphatidylinositol 3-kinase coordinately activates the MEK/ERK and AKT/NFkappaB pathways to maintain osteoclast survival. J Cell Biochem. 2003; 89(1):165–79.
25. Sugatani T, Hruska KA. Akt1/Akt2 and mammalian target of rapamycin/Bim play critical roles in osteoclast differentiation and survival, respectively, whereas Akt is dispensable for cell survival in isolated osteoclast precursors. J Biol Chem. 2005;280(5):3583–9.
26. Matsumoto T, Nagase Y, Iwasawa M, Yasui T, Masuda H, Kadono Y, Nakamura K, Tanaka S. Distinguishing the proapoptotic and antiresorptive functions of risedronate in murine osteoclasts: role of the Akt pathway and the ERK/Bim axis. Arthritis Rheum. 2011;63(12): 3908–17.
27. Buttrick GJ, Wakefield JG. PI3-K and GSK-3: Akt-ing together with microtubules. Cell Cycle. 2008;7(17):2621–5.
28. Allan V, Nathke IS. Catch and pull a microtubule: getting a grasp on the cortex. Nat Cell Biol. 2001;3(10):E226–8.
29. Sharp DJ, Rogers GC, Scholey JM. Roles of motor proteins in building microtubule-based structures: a basic principle of cellular design. Biochim Biophys Acta. 2000;1496(1):128–41.
30. Buttrick GJ, Beaumont LM, Leitch J, Yau C, Hughes JR, Wakefield JG. Akt regulates centrosome migration and spindle orientation in the early Drosophila melanogaster embryo. J Cell Biol. 2008;180(3): 537–48.
31. Onishi K, Higuchi M, Asakura T, Masuyama N, Gotoh Y. The PI3K-Akt pathway promotes microtubule stabilization in migrating fibroblasts. Genes Cells. 2007;12(4):535–46.
32. Mimori-Kiyosue Y, Tsukita S. "Se arch-and-capture" of microtubules through plus-end-binding proteins (+TIPs). J Biochem. 2003;134(3): 321–6.
33. Mimori-Kiyosue Y, Shiina N, Tsukita S. The dynamic behavior of the APC-binding protein EB1 on the distal ends of microtubules. Curr Biol. 2000;10(14):865–8.
34. Polakis P. The adenomatous polyposis coli (APC) tumor suppressor. Biochim Biophys Acta. 1997;1332(3):F127–47.
35. Munemitsu S, Souza B, Muller O, Albert I, Rubinfeld B, Polakis P. The APC gene product associates with microtubules in vivo and promotes their assembly in vitro. Cancer Res. 1994;54(14):3676–81.
36. Smith KJ, Levy DB, Maupin P, Pollard TD, Vogelstein B, Kinzler KW. Wild-type but not mutant APC associates with the microtubule cytoskeleton. Cancer Res. 1994;54(14):3672–5.
37. Wen Y, Eng CH, Schmoranzer J, Cabrera-Poch N, Morris EJ, Chen M, Wallar BJ, Alberts AS, Gundersen GG. EB1 and APC bind to mDia to stabilize microtubules downstream of Rho and promote cell migration. Nat Cell Biol. 2004;6(9):820–30.
38. Green RA, Wollman R, Kaplan KB. APC and EB1 function together in mitosis to regulate spindle dynamics and chromosome alignment. Mol Biol Cell. 2005;16(10):4609–22.
39. Zumbrunn J, Kinoshita K, Hyman AA, Nathke IS. Binding of the adenomatous polyposis coli protein to microtubules increases microtubule stability and is regulated by GSK3 beta phosphorylation. Curr Biol. 2001;11(1):44–9.
40. Berrueta L, Tirnauer JS, Schuyler SC, Pellman D, Bierer BE. The APC-associated protein EB1 associates with components of the dynactin complex and cytoplasmic dynein intermediate chain. Curr Biol. 1999; 9(8):425–8.
41. Chen WS, Xu PZ, Gottlob K, Chen ML, Sokol K, Shiyanova T, Roninson I, Weng W, Suzuki R, Tobe K, Kadowaki T, Hay N. Growth retardation and increased apoptosis in mice with homozygous disruption of the Akt1 gene. Genes Dev. 2001;15(17):2203–8.
42. Kawamura N, Kugimiya F, Oshima Y, Ohba S, Ikeda T, Saito T, Shinoda Y, Kawasaki Y, Ogata N, Hoshi K, Akiyama T, Chen WS, Hay N, Tobe K, Kadowaki T, Azuma Y, Tanaka S, Nakamura K, Chung UI, Kawaguchi H.

Akt1 in osteoblasts and osteoclasts controls bone remodeling. PLoS One. 2007;2(10):e1058.

43. Cho H, Mu J, Kim JK, Thorvaldsen JL, Chu Q. Crenshaw EB 3rd, Kaestner KH, Bartolomei MS, Shulman GI, Birnbaum MJ. Insulin resistance and a diabetes mellitus-like syndrome in mice lacking the protein kinase Akt2 (PKB beta). Science. 2001;292(5522):1728–31.
44. Garofalo RS, Orena SJ, Rafidi K, Torchia AJ, Stock JL, Hildebrandt AL, Coskran T, Black SC, Brees DJ, Wicks JR, McNeish JD, Coleman KG. Severe diabetes, age-dependent loss of adipose tissue, and mild growth deficiency in mice lacking Akt2/PKB beta. J Clin Invest. 2003;112(2):197–208.
45. Peng XD, Xu PZ, Chen ML, Hahn-Windgassen A, Skeen J, Jacobs J, Sundararajan D, Chen WS, Crawford SE, Coleman KG, Hay N. Dwarfism, impaired skin development, skeletal muscle atrophy, delayed bone development, and impeded adipogenesis in mice lacking Akt1 and Akt2. Genes Dev. 2003;17(11):1352–65.

Inui et al. BMC Sports Science, Medicine, and Rehabilitation 2013, 5:10
http://biomedcentral.com/2052-1847/5/10

BMC
Sports Science, Medicine & Rehabilitation

RESEARCH Open Access

Influence of navigation system updates on total knee arthroplasty

Hiroshi Inui*, Shuji Taketomi, Kensuke Nakamura, Seira Takei, Hideki Takeda, Sakae Tanaka and Takumi Nakagawa

Abstract

Background: The purpose of this study was to evaluate the influence of image-free computer-assisted navigation system update on outcome in total knee arthroplasty.

Methods: Thirty-three knees were replaced using the Stryker 3.1 image-free navigation system and 49 knees were replaced using the Stryker 4.0 system. One surgeon took part in all procedures as chief surgeon or first assistant. All patients received the Stryker Scopio NRG CR total knee prosthesis. We compared the accuracy of component positioning measured using radiographs and CT scans, operating time and clinical outcome 1 year after surgery.

Results: The mean hip-knee-ankle, frontal femoral and tibial component angle were 179.8° (ideally implanted 85%), 89.8° (88%), 90.4° (88%) respectively for the 3.1 group and 179.5° (96%), 90.6° (92%), 90.2° (94%) for the 4.0 group. The mean sagittal tibial component angle was 85.5° (82%) for the 3.1 group and 85.6° (92%) for the 4.0 group. The mean rotational femoral and tibial component angle were −0.5° (81%), −0.7° (73%) for the 3.1 group and 0.0° (84%), 0.4° (72%) for the 4.0 group. There were no statistically significant findings with regard to component positioning. Operating time was significantly longer in the 3.1 group (3.1 group: 137 min, 4.1group: 125 min, $P < 0.01$). No significant difference was detected in postoperative clinical outcome.

Conclusion: The navigation system update from Stryker 3.1 to Stryker 4.0 reduced operating time by 12 min. However, there were no statistically significant findings with regard to component positioning and clinical outcome.

Keywords: Image-free navigation, Navigation system update, Total knee arthroplasty, Component positioning, Operating time, Clinical outcome

Background

Total knee arthroplasty (TKA) has become one of the most successful surgical procedures in orthopedic surgery [1,2]. The success of this procedure depends on many factors, including surgical techniques and the design and material of the components. With regard to surgical techniques, implant positioning and soft tissue balancing are very important. Malpositioning of any component can lead to an increased risk of loosening, instability, and pain [3,4]. Restoration of the tibiofemoral angle to within 3° of neutral during TKA is thought to be associated with better outcome [4-7]. The accurate rotational alignment of femoral and tibial components is also considered important [3,8,9].

Computer-assisted navigation systems are designed to increase the accuracy of implantation, and have become much more accepted and prevalent in recent years. Several studies, including a meta-analysis study have demonstrated superior alignment of the components in the coronal plane in navigated compared with conventional implanted TKA, with fewer outliers outside a range of 3° varus or valgus [7,10,11]. Some studies have noted an improvement in the accuracy of rotational alignment using navigation systems [12,13]. However, it is still not clear whether navigation can improve rotational alignment consistently [14,15].

Recently, several software and adapted instrument advancements have been made to further improve the accuracy of total knee component positioning. One recent study demonstrated that advancements in navigation software improved the accuracy of overall mechanical

* Correspondence: hiroshi_inu0707@yahoo.co.jp
Department of Orthopaedic Surgery, Faculty of Medicine, The University of Tokyo, Tokyo, Japan

alignment and several individual component positioning variables; however rotational alignment was not evaluated in that study [16]. Although consistent and accurate rotational positioning is desirable, it remains to be elucidated whether currently available navigation software improves rotational accuracy of placement of components.

Version 2.0 of the Stryker image-free navigation system was first implemented in our institute in January 2007. It was updated to version 3.1 in July 2007 and version 4.0 in January 2009. Molli et al. [16] demonstrated several advancements of the 3.1 system over the 2.0 system, which led to more accurate implant positioning. Several advancements of the 4.0 system have also been noted. Therefore, we hypothesized that this recent navigation system update would improve alignment in TKA and reduce operating time. We evaluated several outcome measurements including overall alignment, individual component positioning, knee score, range of motion, and operating time.

Methods

This study was approved by the institutional review boards of the University of Tokyo (No.2674). All patients provided written informed consent.

Of a total of 109 consecutive primary TKA procedures performed in 93 patients between December 2007 and March 2009, 46 consecutive knees in 33 patients were replaced using the Stryker 3.1 image-free computer navigation system (Stryker Orthopedics, Mahwah, NJ, USA) between December 2007 and December 2008. Sixty-three consecutive knees in 60 patients were replaced using the updated Stryker 4.0 image-free navigation system between January 2008 and March 2009. Thirty-three knees in 30 patients of the Stryker 3.1 group and 49 knees in 48 patients of the Stryker 4.0 group met the inclusion criteria: no major previous orthopedic surgeries (i.e.,, arthroplasty, open reduction-internal fixation procedures, osteotomy), satisfactory full-length standing anteroposterior (AP) and lateral radiographs after operation, complete data entry, and adequate follow up of minimum 1 year. Preoperative variables were recorded including age, sex, body mass index, preoperative diagnosis, mechanical axis, and range of motion. Pre-operative scores were obtained using the Knee Society Score (KSS) [17]. There was no statistically significant difference between the groups in terms of demographic features (Table 1).

Operating procedures

The Stryker Navigation System was used for computer-assisted implantation. The system was image-free and used infrared cameras and light-emitting diodes.

Surgery was performed under a tourniquet. A midvastus approach was used for the varus and neutral knee and a medial parapatellar approach was used for the valgus knee. Bicortical tracker pins were placed into the femoral shaft at the proximal end of the skin incision and the tibial shaft at the distal end of the skin incision. Anatomical landmarks were registered either by the pointer, the validation of which is successful if the deviation between the pointer tip position and the calibration data is 2 mm, or by the calculations of the navigation system to proceed with bone resections and implant positioning. Landmarks comprised the center of the femoral head, the distal femur, the proximal tibia and the ankle, the Whiteside line, the epicondylar axis (lateral epicondyle, medial sulcus), anterior surface of the distal femur cortex, the condylar surfaces of the femur and tibia, and the tibia AP axis.

The center of the femoral head was determined by rotating the femur by rotational calculations. The center of the ankle was represented by a 44%–56% medial to lateral ratio along the transmalleolar axis.

Femoral alignment was aimed at a placement of 90° to the mechanical axis in the frontal plane. In the sagittal plane, anterior notching was avoided by changing the flexion angle and implant size. The femoral rotation axis was defined as the average rotation axis of the transepicondylar axis and the axis perpendicular to the Whiteside line.

For the tibia, alignment was aimed at 90° to the mechanical axis in the frontal plane and 5° of posterior slope in the sagittal plane. The AP axis was aimed along the line from the medial border of the tibia tubercle to the middle of the posterior cruciate ligament [18]. To avoid registration error, we drew the line in blue beforehand.

During femoral and tibial resection, the femur was prepared first. Care was taken to balance the flexion and extension gaps and release any flexion contracture. The patella was everted and resurfaced in all patients. All patients underwent the same postoperative rehabilitation protocol.

There were several advancements of the 4.0 system over the 3.1 system. The number of sensors in the camera was increased from two to three, which facilitated faster and more accurate registration [19]. The automatic implant sizing and positioning system provided accurate implant sizing and aided in avoiding anterior femoral notching (Figure 1a). The navigation template drilling system maintained the registered femoral rotation angle until setting of the 4-in-1 cutting guide and eliminated unnecessary procedures (Figure 1b).

One surgeon (TN) took part in all procedures as chief surgeon or first assistant. All implants used in both groups were Stryker Scopio NRG CR total knee implants. Identical cutting blocks and instrumentation devices were used for all procedures.

Evaluation of post-operative alignment

Alignment in the frontal plane was measured using full-length standing radiograph performed 3–6 months after operation [20]. The mechanical axis of the leg was

Table 1 Pre-operative demographic data

	Version 3.1 group	Version 4.0 group	P-value
Number of patients	33	49	
Sex (female/male)	30/3	43/6	
Diagnosis (OA/others)	31/2	47/2	
Age (years)	75.0 ± 5.0	75.5 ± 5.1	n.s.
Pre-operative KSS	37.9 ± 10.5	36.4 ± 10.1	n.s.
Maximum extension (°)	−9.8 ± 7.2	−11.8 ± 7.1	n.s.
Maximum flexion (°)	120.1 ± 16.4	119.2 ± 15.7	n.s.
Body mass index (kg/m^2)	26.2 ± 3.7	26.1 ± 4.1	n.s.
Pre-operative FTA (°)	185.8 ± 6.9	186.1 ± 9.6	n.s.

defined as the hip–knee–ankle (HKA) angle, which is the angle between the line connecting the center of the hip with that of the knee (the mechanical axis of the femur) and the line connecting the center of the knee with that of the ankle joint (the mechanical axis of the tibia). Frontal alignment of femoral and tibial components (FFC: frontal femoral component angle, FTC: frontal tibial component angle) were also measured by full-length radiograph. The femoral component sagittal alignment and tibial slope (LFC: lateral femoral component angle, LTC: lateral tibial component angle) were measured by lateral radiograph (Figure 2). The LFC angle was measured between the anterior cortex of the distal femur and the shield of the femoral component. The ideal mechanical axis was defined as falling within 3° of 180°, the ideal frontal femoral and tibial component

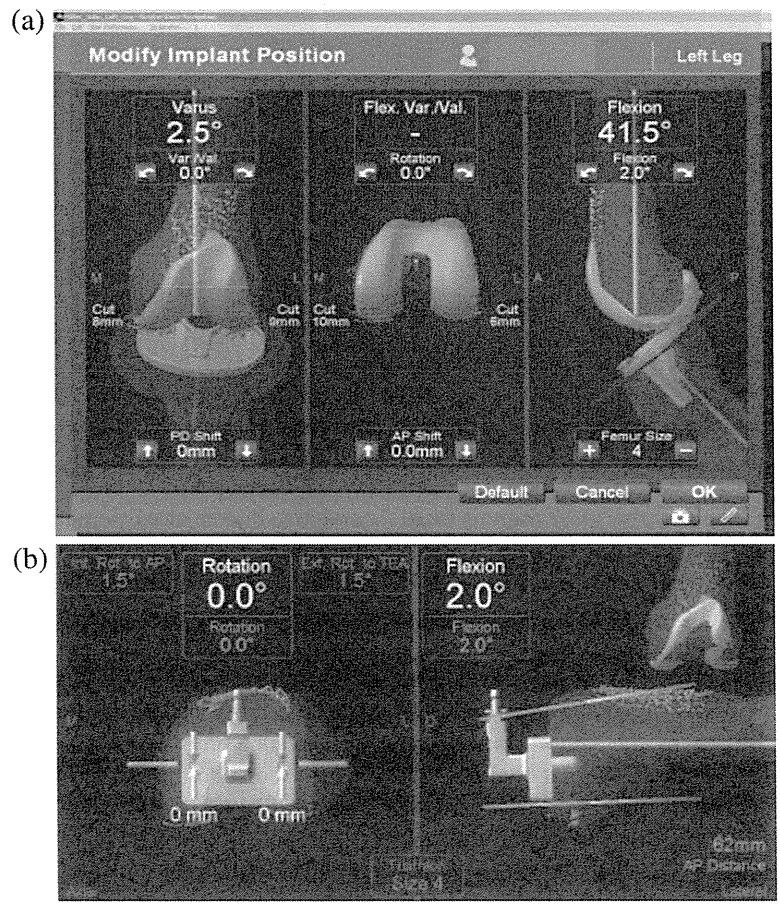

Figure 1 Automatic templating system. a. Automatic implant sizing and positioning system. **b**. Navigation template drilling system, which maintains the registered femoral rotation angle until setting of the 4-in-1 cutting guide.

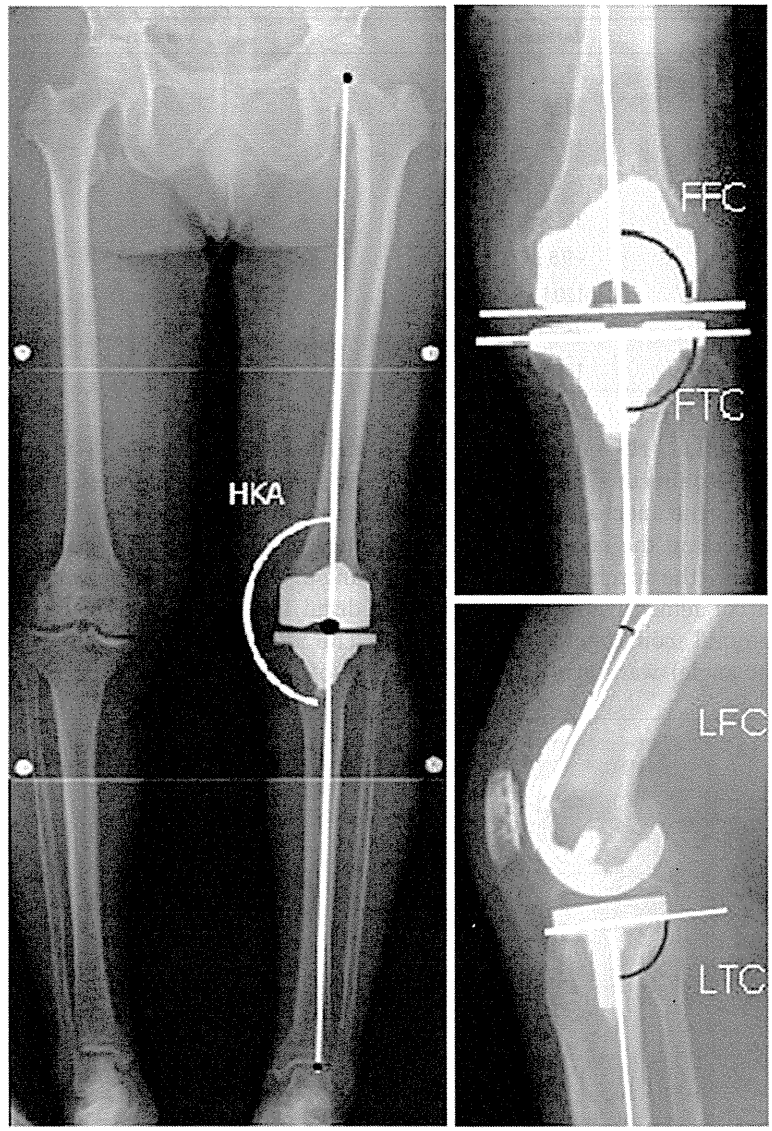

Figure 2 Evaluation of coronal and sagittal alignment by full-length standing and lateral radiography.

angles were within 2° of 90°, and the ideal sagittal tibial angle was within 2° of 85° [11,12,16]. The sagittal femoral component angle was determined separately in each individual through minute change in flexion angle and implant size for avoiding anterior notching.

Twenty-six knees in the version 3.1 group and 25 patients in the version 4.0 group were assessed by axial CT imaging. Rotational alignment of the femoral and tibial components was evaluated by CT. The rotational femoral component angle was defined as the angle between the line through the center of both fixation pegs and the surgical epicondylar axis (Figure 3a). The rotational tibial component angle was defined as the angle between the line connecting the medial border of the tibial tuberosity with the center of the posterior concavity of the tibial tray and the line formed perpendicular to the line along the posterior edge of the tibial tray [18] (Figure 3b, c). The ideal rotational femoral and tibial components angles were defined as falling within 3° of 90° [12].

All radiographs and CT scans were measured twice at 3-month intervals by one observer (HI), who was not part of the operating team and who had no knowledge of the patients.

Operating time was collected from records of intraoperative information. Postoperative KSSs and range of motion were recorded 1 year after surgery.

Statistical analysis

Data were analyzed using the EXCEL statistics 2008 (SSRI Co., LTD., Tokyo, Japan) software package for Microsoft Windows. Data were checked for normality of

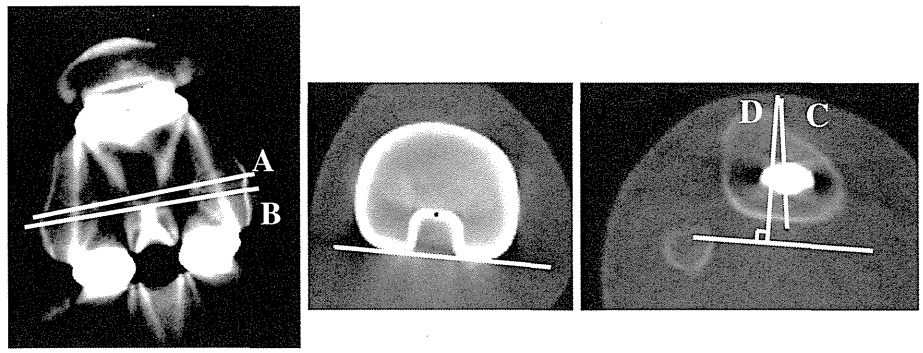

Figure 3 Measurement of rotational alignment. a. RFC angle is defined as the angle between **A** and **B**. **A**: Line through the center of both fixation pegs. **B**: Surgical epicondylar line. **b**. White line: along the posterior edge of the tibial tray. Black dot: center of the posterior concavity of the tibial tray. **c**. RTC angle is defined as the angle between **C** and **D**. **C**: Line connecting the medial border of the tibial tuberosity with the black dot. **D**: Line perpendicular to the white line.

distribution using the Kolmogorov–Smirnov test. For normally distributed data Student's t-test was used to compare the two groups. For data not normally distributed, the Mann–Whitney U-test was applied. Fisher's exact probability test was used to compare the rate of optimally implanted components between the two groups. All significance tests were two-tailed, and a significance level of $P < 0.05$ was used for all tests.

Results

The average postoperative HKA angle was 179.8° ± 2.6° [mean ± standard deviation (SD), range: 174°–185°] for the 3.1 group and 179.5° ± 1.5° (range: 176°–184°) for the 4.0 group. With regard to outliers, 28 cases (84.8%) were implanted ideally (within 3° of 180°) in the 3.1 group, whereas 47 cases (96.0%) were implanted ideally in the 4.0 group. There was not a statistically significant improvement in the more advanced navigation system group (P =0.11) (Figure 4). The average FFC angle was 89.8° ± 1.6° (range: 87°–94°) for the 3.1 group and 90.6° ± 1.3° (range: 87°–93°) for the 4.0 group. The average FTC angle was 90.4° ± 1.7° (range: 86°–95°) for the 3.1 group and 90.2° ± 1.3° (range: 87°–93°) for the 4.0 group. The average LFC angle was 5.8° ± 2.7° (range: 0°–12°) for the 3.1 group and 6.7° ± 3.1° (range: 1°–13°) and there was no case of anterior femoral notching in either group. The average LTC angle was 85.5° ± 2.3° (range: 78°–89°) for the 3.1 group and 85.6° ± 1.6° (range: 82°–89°) for the 4.0 group. For the individual component positioning on radiographs, there were no statistically significant findings (Table 2).

The mean RFC angle was −0.5° ± 2.3° (4° of external rotation to 5° of internal rotation) for the 3.1 group and 0.0° ± 2.1° (4° of external rotation to 5° of internal rotation) for the 4.0 group. Ideal rotational femoral angle was obtained in 80.7% (21 of 26knees) in the 3.1 group and 84.0% (21 of 25 knees) in the 4.0 group. The mean RTC angle was −0.7° ± 3.1° (7° of external rotation to 7° of internal rotation) in the 3.1 group and 0.4° ± 3.3° (7° of external rotation to 5° of internal rotation) in the 4.0 group. Ideal rotational tibial angle was obtained in 73.1% (19 of 26knees) in the 3.1 group and in 72.0% (18 of 25 knees) in the 4.0 group (Table 2). No statistically significant improvement with regard to the rotational alignment was observed. Intra-observer differences were as follows: HKA 0.2° ± 0.4°, FFC 0.2° ± 0.4°, FTC 0.2° ± 0.4°, LFC 0.5° ± 1.0°, LTC 0.4° ± 0.6°, RFC 0.4° ± 0.5° and RTC 0.7° ± 0.7°.

Mean post-operative KSS was 90.1 (range: 72–99) for the 3.1 group and 91.1 (72–100) for the 4.0 group. Mean post-operative functional score was 78.8 (40–100) for the 3.1 group and 77.9 (30–100) for the 4.0 group. No

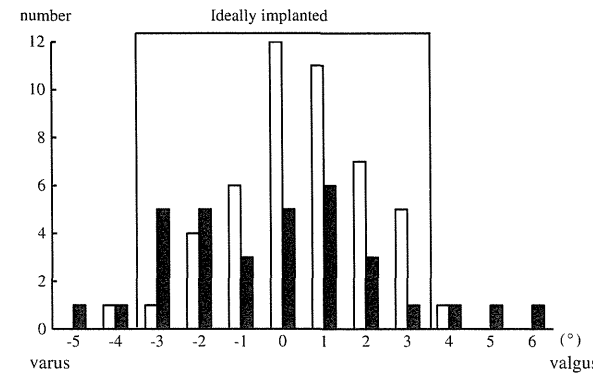

Figure 4 Distribution of the postoperative hip-knee-ankle angle (=leg mechanical axis). Box represents ideal alignment (± 3° of biomechanical neutral).

Table 2 Postoperative component alignment

(A) Mean degrees of individual component alignment (± SD)			
	Version 3.1 group	Version 4.0 group	P- value
Radiograph			
Number	33	49	
HKA (°)	179.8 ± 2.6	179.5 ± 1.7	n.s
FFC (°)	90.2 ± 1.6	90.6 ± 1.3	n.s
FTC (°)	89.5 ± 1.8	90.2 ± 1.3	n.s
LTC (°)	85.5 ± 2.4	85.6 ± 1.6	n.s
LFC (°)	5.8 ± 2.8	6.7 ± 3.1	n.s
CT			
Number	26	25	
RFC (°)	−0.5 ± 2.3	0.2 ± 2.2	n.s
RTC (°)	−0.2 ± 3.4	1.1 ± 3.4	n.s
(B) Ideal implantations			
Radiograph			
HKA	84.8% (28/33)	95.9% (47/49)	n.s
FFC	87.8% (29/33)	91.8% (45/49)	n.s
FTC	87.8% (29/33)	93.9% (46/49)	n.s
LTC	81.8% (27/33)	91.8% (45/49)	n.s
CT			
RFC	80.7% (21/26)	84.0% (21/25)	n.s
RTC	73.1% (19/26)	72.0% (17/25)	n.s

significant difference was detected in these values between the two groups.

Range of motion did not differ between the groups 1 year after surgery.

Operating time was significantly longer in the 3.1 group, with a median duration of 137 minutes (range: 99–209) compared with 125 minutes (range: 90–188) for the 4.0 group ($P < 0.01$) (Table 3).

Discussion

In previous studies, increased rates of early aseptic loosening of TKA were in large part attributed to malalignment of the mechanical axis [4,21]. The tolerable range of mechanical axis deviation after TKA is still under discussion [22]. However, several authors report superior long-term survivorship of TKA with a leg mechanical axis within 3° of the ideal angle [4,21].

In the current study, implants were placed within ± 3° of the desired angle in 96% of the 4.0 group. There have been many publications on computer navigation assisted TKA and its accuracy in terms of the mechanical axis. Our results regarding the accuracy of the mechanical axis using the most recent navigation system (4.0) seemed comparable or superior to those of other studies [11,23]. Molli et al. [16] showed that an earlier navigation system update (from Stryker 2.0 to Stryker 3.1) improved the accuracy of TKA. Several software advancements occurred between Stryker 2.0 and Stryker 3.0 such as a different algorithm for calculating the center of the ankle joint and the addition of "reactive workflow" software. However, our study represented the 4.0 group did not show a statistically significant advantage over the 3.1 group with regard to alignment. This may be quite natural because of the same algorithm for calculation, the same "work flow" software, and the same landmarks to determine the mechanical axis.

With regard to accuracy of the rotational alignment, few studies have demonstrated an improvement with computer-assisted navigation compared with conventional methods [12,13,24]. For femoral rotation, many authors have reported variability in the identification of the transepicondylar axis [25,26]. Yau et al. [26] found that the maximum combined error was 8.2° with 5.3° at the medial femoral epicondyle and 2.9° at the lateral in the transepicondylar axis. Some authors have speculated that this variability is caused by soft tissue coverage [27,28]. However, in a cadaveric study, Siston et al. [29] demonstrated high variability even after all soft tissues had been stripped. Mizu-uchi et al. [12] demonstrated that 89.3% of femoral components were implanted within 3° of ideal rotational alignment in the CT navigation group, whereas 66.7% were implanted ideally in the conventional group. They concluded the CT-based navigation system significantly improved the accuracy of femoral rotational alignment. In the current study 82.3% of femoral components [42 of 51 knees, version 3.1: 80.8% (21/26), version 4.0: 84.0% (21/25)] were implanted ideally. Although no comparison was made with a conventional group in our study, this result is superior to those mentioned in previous studies using conventional techniques [12,15]. Stock et al. [13] noted improvement using a navigation system that established

Table 3 Intra- and post-operative observations

	3.1 group (N = 33)	4.0 group (N = 49)	P-value
Operating time (min)	136.9 ± 22.4	124.9 ± 22.1	0.008
Post-operative (1 year)			
KSS	90.1 ± 6.4	91.1 ± 6.2	n.s
Maximum extension (°)	−1.4 ± 3.2	−2.0 ± 3.4	n.s
Maximum flexion (°)	113.1 ± 11.8	116.6 ± 10.4	n.s

femoral rotational alignment by averaging the angles determined by Whiteside's line and the transepicondylar axis. The femoral implant was ideally located in over 80% of cases in the current study, possibly because the navigation system used here determines the femoral axis in the same manner. We observed no significant improvement using the system update (from Stryker 3.0 to 4.1).

For tibial rotation, it is much more difficult to define the AP axis, which is the line from the medial border of the tibial tuberosity to the center of the posterior cruciate ligament. In addition, there is no consensus on how to measure rotational alignment of the tibial component. Aiming for the posterior cruciate ligament during surgery is relatively easy, but this structure is difficult to determine on CT scans after implantation. Therefore, we used a line from the medial border of the tibial tuberosity to the center of the posterior concavity of the tibial tray as a reference for rotational alignment. In Mizu-uchi et al. [12], 78.6% of the tibial components were implanted within 3° of the ideal rotational alignment in the CT navigation group, whereas 46.2% of the tibial components were implanted ideally in the conventional group. The CT-based navigation system improved the accuracy of tibial rotational alignment significantly in that study. In this study, 72.5% of the tibial components [37 in 51 knees, version 3.1: 73.1% (19/26), version 4.0: 72.0% (18/25)] were implanted ideally, which is comparable to previous reports [7,12,30]. However, as is often reported in previous studies, the accuracy of the tibial rotational alignment is inferior to that of the frontal, sagittal and femoral rotational alignments [12,30].

The accuracy of the rotational alignment the CT-based navigation reached is ideally enough for us to urge to use it. However, taking the demerits of the additional cost and radiation dose associated with CT into consideration, what we have to do is to improve the accuracy using CT-free navigation system. To achieve more accurate rotational alignment, not only further refinements in navigation technology but also more careful and precise registration will be necessary. Additional reference lines such as a posterior condylar line and a trochlear line may reduce the registration error and improve femoral rotational accuracy [29,31]. Improvements in rotational accuracy may lead to a better postoperative outcome [32].

The navigation system update from Stryker 3.1 to Stryker 4.0 reduced operating time by 12 min. Advancements in navigation software and specific adapted instruments may account for this improvement. One of the disadvantages of using navigation systems in TKA is said to be the increased operating time. In previous studies, time for computer-assisted surgical procedures increased by 8–16 min [16,23,33,34]. Navigation system update may have overcome this problem to some extent.

There were some limitations to the current study. One limitation is that surgery in the two groups was performed at different time periods. Some studies have showed that the learning curve affects operating time and alignment in navigated surgery, especially in early cases. Twenty to thirty implantations were said to be necessary before surgeons were accustomed to the navigation system and the average operating time reached a plateau [35,36]. At our institute, 30 implantations using the image-free navigation system (Stryker 2.0 and 3.1) had been performed by the end of November 2007. Therefore, we think our result would not have been affected by the learning curve. Another limitation is the relatively small number of patients. For instance, with regard to HKA angle, 85% were implanted ideally in the 3.1 group, whereas 96% were implanted ideally in the 4.0 group. Indeed there was not a statistically significant improvement (P =0.11). However, we think there was at least a tendency of improvement and further study may change our conclusion.

Conclusion

In conclusion, the navigation system update from Stryker 3.1 to Stryker 4.0 reduced operating time by 12 min. However, there were no statistically significant findings with regard to component positioning and clinical outcome.

Competing interests

The authors declare that they have no competing interests.

Authors' contributions

HI designed the study and wrote the draft of the manuscript. ST, KN and HT provided logistical support. ST and TN participated in the design of the study and performed the statistical analysis. ST conceived the study, and participated in its design and coordination. All authors read and approved the final manuscript.

Received: 31 August 2012 Accepted: 12 April 2013
Published: 2 May 2013

References

1. Vessely MB, Whaley AL, Harmsen WS, Schleck CD, Berry DJ: **Long-term survivorship and failure modes of 1000 cemented condylar total knee arthroplasties.** *Clin Orthop Relat Res* 2006, **452**:28–34.
2. Lutzner J, Gunther KP, Kirschner S: **Functional outcome after computer-assisted versus conventional total knee arthroplasty: a randomized controlled study.** *Knee Surg Sports Traumatol Arthrosc* 2010, **18**:1339–1344.
3. Nicoll D, Rowley DI: **Internal rotational error of the tibial component is a major cause of pain after total knee replacement.** *J Bone Joint Surg Br* 2010, **92**:1238–1244.
4. Jeffery RS, Morris RW, Denham RA: **Coronal alignment after total knee replacement.** *J Bone Joint Surg Br* 1991, **73**:709–714.
5. Werner FW, Ayers DC, Maletsky LP, Rullkoetter PJ: **The effect of valgus/varus malalignment on load distribution in total knee replacements.** *J Biomech* 2005, **38**:349–355.
6. Berger RA, Crossett LS, Jacobs JJ, Rubasg HE: **Malrotation causing patellofemoral complications after total knee arthroplasty.** *Clin Orthop Relat Res* 1998, **356**:144–153.
7. Matziolis G, Krocker D, Weiss U, Tohtz S, Perka C: **A prospective, randomized study of computer-assisted and conventional total knee arthroplasty. Three-dimensional evaluation of implant alignment and rotation.** *J Bone Joint Surg Am* 2007, **89**:236–243.
8. Verlinden C, Uvin P, Labey L, Luyckx JP, Bellemans J, Vandenneucker H: **The influence of malrotation of the femoral component in total knee**

replacement on the mechanics of patellofemoral contact during gait: an in vitro biomechanical study. *J Bone Joint Surg Br* 2010, **92**:737–742.
9. Wasielewski RC, Galante JO, Leighty RM, Natarajan RN, Rosenberg AG: **Wear patterns on retrieved polyethylene tibial inserts and their relationship to technical considerations during total knee arthroplasty.** *Clin Orthop Relat Res* 1994, **299**:31–43.
10. Longstaff LM, Sloan K, Stamp N, Scaddan M, Beaver R: **Good alignment after total knee arthroplasty leads to faster rehabilitation and better function.** *J Arthroplasty* 2009, **24**:570–578.
11. Mason JB, Fehring TK, Estok R, Banel D, Fahrbach K: **Meta-analysis of alignment outcomes in computer-assisted total knee arthroplasty surgery.** *J Arthroplasty* 2007, **22**:1097–1106.
12. Mizu-uchi H, Matsuda S, Miura H, Okazaki K, Akasaki Y, Iwamoto Y: **The evaluation of post-operative alignment in total knee replacement using a CT-based navigation system.** *J Bone Joint Surg Br* 2008, **90**:1025–1031.
13. Stockl B, Noquler M, Rosiek R, Fischer M, Krismer M, Kessler O: **Navigation improves accuracy of rotational alignment in total knee arthroplasty.** *Clin Orthop Relat Res* 2004, **426**:180–186.
14. Bauwens K, Matthes G, Wich M, Gebhard F, Hanson B, Ekkernkamp A, Stengel D: **Navigated total knee replacement. A meta-analysis.** *J Bone Joint Surg Am* 2007, **89**:261–269.
15. Kim YH, Kim JS, Yoon SH: **Alignment and orientation of the components in total knee replacement with and without navigation support: a prospective, randomised study.** *J Bone Joint Surg Br* 2007, **89**:471–476.
16. Molli RG, Anderson KC, Buehler KC, Markel DC: **Computer-assisted navigation software advancements improve the accuracy of total knee arthroplasty.** *J Arthroplasty* 2011, **26**:432–438.
17. Insall JN, Dorr LD, Scott RD, Scott WN: **Rationale of the knee society clinical rating system.** *Clin Orthop Relat Res* 1989, **248**:13–14.
18. Akagi M, Oh M, Nonaka T, Tsujimoto H, Asano T, Hamanisi C: **An anteroposterior axis of the tibia for total knee arthroplasty.** *Clin Orthop Relat Res* 2004, **420**:213–219.
19. Elfring R, de la Fuente M, Randermacher K: **Assessment of optical localizer accuracy for computer aided surgery systems.** *Comput Aided Surg* 2010, **15**:1–12.
20. Hauschild O, Konstantinidis L, Baumann T, Niemeyer P, Suedkamp NP, Helwig P: **Correlation of radiographic and navigated measurements of TKA limb alignment: a matter of time?** *Knee Surg Sports Traumatol Arthrosc* 2010, **18**:1317–1322.
21. Ritter MA, Herbst SA, Keating EM, Faris PM, Meding JB: **Long-term survival analysis of a posterior cruciate-retaining total condylar total knee arthroplasty.** *Clin Orthop Relat Res* 1994, **309**:136–145.
22. Parratte S, Pagnano MW, Ttousdale RT, Berry DJ: **Effect of postoperative mechanical axis alignment on the fifteen-year survival of modern, cemented total knee replacements.** *J Bone Joint Surg Am* 2010, **92**:2143–2149.
23. Bathis H, Perlick L, Tingart M, Luring C, Zurakowski D, Grifka J: **Alignment in total knee arthroplasty. A comparison of computer-assisted surgery with the conventional technique.** *J Bone Joint Surg Br* 2004, **86**:682–687.
24. Chauhan SK, Clark GW, Lloyd S, Scott RG, Breidahl W, Sikorski JM: **Computer-assisted total knee replacement. A controlled cadaver study using a multi-parameter quantitative CT assessment of alignment (the Perth CT protocol).** *J Bone Joint Surg Br* 2004, **86**:818–823.
25. Kinzel V, Ledger M, Shakespeare D: **Can the epicondylar axis be defined accurately in total knee arthroplasty?** *Knee* 2005, **12**:293–296.
26. Yau WP, Leung A, Chiu KY, Tang WM, Ng TP: **Intraobserver errors in obtaining visually selected anatomic landmarks during registration process in nonimage-based navigation-assisted total knee arthroplasty: a cadaveric experiment.** *J Arthroplasty* 2005, **20**:591–601.
27. Arima J, Whiteside LA, McCarthy DS, White SE: **Femoral rotational alignment, based on the anteroposterior axis, in total knee arthroplasty in a valgus knee. A technical note.** *J Bone Joint Surg Am* 1995, **77**:1331–1334.
28. Jenny JY, Boeri C: **Low reproducibility of the intra-operative measurement of the transepicondylar axis during total knee replacement.** *Acta Orthop Scand* 2004, **75**:74–77.
29. Siston RA, Patel JJ, Goodman SB, Delp SL, Giori NJ: **The variability of femoral rotational alignment in total knee arthroplasty.** *J Bone Joint Surg Am* 2005, **87**:2276–2280.
30. Ikeuchi M, Yamanaka N, Okanoue Y, Ueta E, Tani T: **Determining the rotational alignment of the tibial component at total knee replacement: a comparison of two techniques.** *J Bone Joint Surg Br* 2007, **89**:45–49.
31. Won YY, Cui WQ, Baek MH, Yun TB, Han SH: **An additional reference axis for determining rotational alignment of the femoral component in total knee arthroplasty.** *J Arthroplasty* 2007, **22**:1049–1053.
32. Czurda T, Fennema P, Baumgartner M, Ritschl P: **The association between component malalignment and post-operative pain following navigation-assisted total knee arthroplasty: results of a cohort/nested case–control study.** *Knee Surg Sports Traumatol Arthrosc* 2010, **18**:863–869.
33. Jenny JY, Clemens U, Kohler S, Kiefer H, Konermann W, Miehlke RK: **Consistency of implantation of a total knee arthroplasty with a non-image-based navigation system: a case–control study of 235 cases compared with 235 conventionally implanted prostheses.** *J Arthroplasty* 2005, **20**:832–839.
34. Tingart M, Luring C, Bathis H, Beckmann J, Grifka J, Perlick L: **Computer-assisted total knee arthroplasty versus the conventional technique: how precise is navigation in clinical routine?** *Knee Surg Sports Traumatol Arthrosc* 2008, **16**:44–50.
35. Jenny JY, Miehlke RK, Giurea A: **Learning curve in navigated total knee replacement. A multi-centre study comparing experienced and beginner centres.** *Knee* 2008, **15**:80–84.
36. Smith BR, Deakin AH, Baines J, Picard F: **Computer navigated total knee arthroplasty: the learning curve.** *Comput Aided Surg* 2010, **15**:40–48.

doi:10.1186/2052-1847-5-10
Cite this article as: Inui *et al.*: **Influence of navigation system updates on total knee arthroplasty.** *BMC Sports Science, Medicine, and Rehabilitation* 2013 5:10.

Chikuda et al. BMC Musculoskeletal Disorders 2013, 14:173
http://www.biomedcentral.com/1471-2474/14/173

BMC
Musculoskeletal Disorders

RESEARCH ARTICLE Open Access

Impact of age and comorbidity burden on mortality and major complications in older adults undergoing orthopaedic surgery: an analysis using the Japanese diagnosis procedure combination database

Hirotaka Chikuda[1*], Hideo Yasunaga[2], Hiromasa Horiguchi[2], Katsushi Takeshita[1], Shurei Sugita[1], Shuji Taketomi[1], Kiyohide Fushimi[3] and Sakae Tanaka[1]

Abstract

Background: The purpose of this study was to examine how complications in older adults undergoing orthopaedic surgery vary as a function of age, comorbidity, and type of surgical procedure.

Methods: We abstracted data from the Japanese Diagnosis Procedure Combination database for all patients aged ≥ 50 who had undergone cervical laminoplasty, lumbar decompression, lumbar arthrodesis, or primary total knee arthroplasty (TKA) between July 1 and December 31 in the years 2007 to 2010. Outcome measures included all-cause in-hospital mortality and incidence of major complications. We analyzed the effects of age, sex, comorbidities, and type of surgical procedure on outcomes. Charlson comorbidity index was used to identify and summarize patients' comorbid burden.

Results: A total of 107,104 patients were identified who underwent cervical laminoplasty (16,020 patients), lumbar decompression (31,605), lumbar arthrodesis (18,419), or TKA (41,060). Of these, 17,339 (16.2%) were aged 80 years or older. Overall, in-hospital death occurred in 121 patients (0.11%) and 4,448 patients (4.2%) had at least one major complication. In-hospital mortality and complication rates increased with increasing age and comorbidity. A multivariate analysis showed mortality and major complications following surgery were associated with advanced age (aged ≥ 80 years; odds ratios 5.88 and 1.51), male gender, and a higher comorbidity burden (Charlson comorbidity index ≥ 3; odds ratio, 16.5 and 5.06). After adjustment for confounding factors, patients undergoing lumbar arthrodesis or cervical laminoplasty were at twice the risk of in-hospital mortality compared with patients undergoing TKA.

Conclusions: Our data demonstrated that an increased comorbid burden as measured by Charlson comorbidity index has a greater impact on postoperative mortality and major complications than age in older adults undergoing orthopaedic surgery. After adjustment, mortality following lumbar arthrodesis or cervical laminoplasty was twice as high as that in TKA. Our findings suggest that an assessment of perioperative risks in elderly patients undergoing orthopaedic surgery should be stratified according to comorbidity burden and type of procedures, as well as by patient's age.

Keywords: Orhopaedic surgery, Spine surgery, Arthroplasty, Complication, Mortality, Database, Charlson comorbidity index, Elderly patients

* Correspondence: chikuda-tky@umin.ac.jp
[1]Department of Orthopaedic Surgery, Faculty of Medicine, The University of Tokyo, 7-3-1 Hongo, Bunkyo-ku, Tokyo 113-8655, Japan
Full list of author information is available at the end of the article

Background

Orthopaedic surgery for degenerative spine or limb joints is widely performed with the aim of improving patients' quality of life. In the United States, about 400,000 spinal arthrodesis and 600,000 total knee arthroplasty (TKA) operations are completed annually [1,2]. Orthopaedic surgery for elderly patients, even octogenarians and nonagenarians, is becoming more common as the population ages. This trend is particularly evident in Japan, where 23% of the population are 65 years or older [3,4].

Despite the rapid increase of surgical treatment in elderly patients, the impact of advanced age on the risk arising from orthopaedic surgery is not fully understood. Although age has long been considered as a major risk factor for perioperative mortality and morbidity, chronological age is not the sole determinant of surgical risk. Risk factors vary considerably among individuals and depend on multiple variables including severity of disease, comorbid conditions, and type of surgical procedure. Further understanding of each factor's contribution would allow surgeons to better evaluate perioperative risk to elderly patients. However, few large studies, in particular those using a national database, has examined this issue [1,5-10].

In this analysis of nationwide inpatient claim data, we investigated mortality and morbidity in older adults undergoing one of the following operations: cervical laminoplasty; lumbar decompression; lumbar arthrodesis; and primary TKA to examine how complications vary as a function of age, comorbid conditions, and type of surgical procedure.

Methods

Data source

The Diagnosis Procedure Combination (DPC) is a case-mix patient classification system launched in 2002 by the Ministry of Health, Labour and Welfare of Japan, and linked with a lump-sum payment system [11-14]. All 82 university teaching hospitals are obliged to use this system, but adoption by community hospitals is voluntary. The DPC Research Group surveys participating hospitals between July 1 and December 31 each year in collaboration with the Ministry of Health, Labour and Welfare. In 2010, 926 hospitals participated and provided data for 2.9 million patients, approximately 45% of all inpatient admissions to acute care hospitals in Japan. The database includes the International Classification of the Diseases 10th Revision (ICD-10) codes for primary and secondary diagnoses; comorbid conditions that existed at admission; and complications that occurred after admission. To optimize the accuracy of the recorded diagnoses, physicians in charge are obliged to record the diagnoses with reference to medical charts.

The Institutional Review Board at The University of Tokyo approved the study design and waived informed consent because the data is anonymous.

Patients

We included all patients aged 50 years or older who had undergone one of the following operations from 2007 to 2010: cervical laminoplasty, lumbar decompression, lumbar arthrodesis, and primary TKA. These procedures were chosen because they are predominantly performed for degenerative conditions commonly seen in the elderly. Although these procedures might be conducted in an urgent manner, this study did not exclude emergency cases. We excluded total hip arthroplasty (THA) from our analysis because of demographic and etiologic differences; the majority of Japanese patients present with osteoarthritis secondary to dysplasia of the hip joint, which is not necessarily the case in other parts of the world.

The variables abstracted from the DPC database were: age, sex, comorbid conditions that existed at admission, surgical site, length of stay, and postoperative adverse outcomes. To evaluate the impact of multiple comorbidities, we used Charlson comorbidity index (CCI) base on Quan's protocol [15,16], a weighted index that takes into account the number and the seriousness of comorbid conditions. In calculation of the CCI, patients' comorbid conditions are classified into following 17 categories: myocardial infarction; congestive heart failure; peripheral vascular disease; cerebrovascular disease; dementia; chronic pulmonary disease; peptic ulcer diease; mild liver disease; diabetes without chronic complication; diabetes with chronic complication; hemiplesia or paraplegia; renal disease; any malignancy, including leukemia and lymphoma; moderate or severe liver disease; metastatic solid tumor; and AIDS/HIV. Each condition is assigned a score of 1, 2, 3, or 6, depending on the risk of dying associated with the condition. Scores are then summed to provide a total score of the CCI. In the present study, coded comorbidities in the DPC database were converted to designated points according to Quan's protocol.

Outcomes

Primary outcomes included in-hospital death or any of the following complications: surgical site infection (ICD10 code: T793, T814), sepsis (A40, A41), cardiac events (acute coronary events [I21-I24] or heart failure [I50]), respiratory complications (pneumonia [J12-J18], post procedural respiratory disorders [J95] or respiratory failure [J96]), pulmonary embolism (I26), stroke (cerebral infarction or hemorrhage [I60-I64]), acute renal failure [N17].

Statistical analysis

We used analysis of variance or Kruskal-Wallis tests to compare continuous data; Chi-square tests to compare categorical data; Fisher's exact test to compare in-hospital mortality and major complication rates between subgroups; logistic regression to analyze concurrent effects of factors on the occurrence of in-hospital deaths and postoperative

complications, and a generalized estimating equation to adjust for the clustering of patients within hospitals. In the regressions, in-hospital deaths and postoperative complications were modeled as functions of age, sex, CCI, and surgical procedure [17]. The threshold for significance was < 0.05.

Results

A total of 107,104 patients were identified (45,044 men and 62,060 women; mean ± SD age, 70.1 ± 10.7 years): cervical laminoplasty (16,020 patients); lumbar decompression (31,605); lumbar arthrodesis (18,419); or primary TKA (41,060). Of these, 17,339 (16.2%) were aged ≥ 80 years. Diabetes was the most common comorbid condition that existed at admission (found in 16.0% of the patients) followed by chronic pulmonary disease (2.6%), chronic renal failure (1.9%), malignancy (1.7%), and congestive heart failure (1.6%). Table 1 shows the characteristics of the patients according to surgical procedures.

One-hundred and twenty-one patients died in-hospital following surgery (0.11%), and 4,448 patients (4.2%) experienced at least one major complication (Table 2). The most common major complication was surgical site infection (about 2% of patients) followed by cardiac events and respiratory complications. As expected, in-hospital mortality and complication rate increased with age and comorbid burden (Table 2). Patient receiving cervical laminoplasty showed the highest mortality (0.20%) and major complication rate (4.7%).

Mortality and major complication following surgery were associated with advanced age (aged ≥ 80 years; odds ratios [OR], 5.88 and 1.51 respectively), male gender, and increasing comorbidity (CCI ≥ 3; OR, 16.5, and 5.06 respectively) (Table 3). We note the risk of in-hospital death following lumbar arthrodesis or cervical laminoplasty was twice that in TKA.

Discussion

Overall, our results confirmed that mortality following current orthopaedic surgery was low (0.11%). Although these results support previous reports [18], there was a marked difference in risk profile among patient subgroups. The multivariate analysis showed that postoperative mortality and morbidity were modestly associated with advanced age and strongly with the comorbidity burden as measured by the CCI. An increased CCI was the greatest risk factor for both in-hospital mortality and the occurrence of major complications. In addition, the use of lumbar arthrodesis and cervical laminoplasty were associated with increased risk of in-hospital mortality compared with TKA.

Strengths and weaknesses of the study

This study is the largest (study population of 107,104) that analyzes the risks associated with current orthopaedic surgery in older adults. The DPC database is a large administrative database similar to National Inpatient Sample in the United States, and the data allows nationwide investigation and comparison of mortality and morbidity between stratified subgroups. In addition, the DPC database allows us to assess perioperative complications by differentiating comorbidities at admission and complications after admission.

In common with other studies using administrative data, a degree of misclassification or underreporting

Table 1 Characteristics of the study population according to surgical procedures

	Overall	Cervical laminoplasty	Lumbar decompression	Lumbar arthrodesis	Total knee arthroplasty	p
	(n = 107,104)	(n = 16,020)	(n = 31,605)	(n = 18,419)	(n = 41,060)	
Age, years; mean [SD]	70.1 [10.7]	66.2 [11.6]	68.9 [11.3]	65.7 [12.1]	74.6 [6.9]	< 0.001
≤ 64	25,927 (24.2)	6,534 (40.8)	8,898 (28.2)	6,976 (37.9)	3,519 (8.6)	
65–79	63,838 (59.0)	7,678 (47.9)	18,166 (57.5)	10,060 (54.6)	27,394 (68.0)	
≥ 80	17,339 (16.2)	1,808 (11.3)	4,541 (14.4)	1,383 (7.5)	9,607 (23.4)	
Sex						
Men	45,044 (42.1)	11,050 (69.0)	18,735 (59.3)	8,456 (45.9)	6,803 (16.6)	< 0.001
Women	62,060 (57.9)	4,970 (31.0)	12,870 (40.7)	9,963 (54.1)	34,257 (83.4)	
Charlson comorbidity index						
0	68,931 (64.4)	9,518 (59.4)	20,234(64.0)	11,971 (65.0)	27,208 (66.3)	< 0.001
1	24,068 (22.5)	3,481 (21.7)	7,060(22.3)	3,825 (20.8)	9,702 (23.6)	
2	9,656 (9.0)	1,885 (11.8)	2,928(9.3)	1,747 (9.5)	3,096 (7.5)	
≥ 3	4,449 (4.2)	1,136 (7.1)	1,383(4.4)	876 (4.8)	1,054 (2.6)	
Postoperative length of stay, day, median [IQR]	21 [15–30]	18 [14–26]	15 [12-21]	20 [15–28]	27 [21–36]	< 0.001

SD standard deviation, *IQR* interquartile range.

Table 2 Mortality and major complications following surgery according to age groups

	Cervical laminoplasty (n = 16,020)	Lumbar decompression (n = 31,605)	Lumbar arthrodesis (n =18,419)	Total knee arthroplasty (n = 41,060)	p
Inhospital death, n (%)	32 (0.20)	35 (0.11)	27 (0.15)	27 (0.066)	< 0.001
Age ≤ 64 years	5(0.077)	4 (0.045)	3 (0.043)	1 (0.028)	
65–79	17(0.22)	20 (0.11)	17 (0.17)	15 (0.055)	
≥ 80	10(0.55)	11 (0.24)	7 (0.51)	11 (0.11)	
Postoperative complications, n (%)					
Surgical site infection	320 (2.0)	511 (1.6)	362 (2.0)	636 (1.5)	< 0.001
Sepsis	25 (0.16)	53 (0.17)	53 (0.29)	61 (0.15)	0.002
Cardiac events	279 (1.7)	508 (1.6)	302 (1.6)	677 (1.6)	0.754
Respiratory complications	96 (0.60)	104 (0.33)	88 (0.48)	196 (0.48)	< 0.001
Pulmonary embolism	16 (0.10)	31 (0.10)	31 (0.17)	167 (0.41)	< 0.001
Stroke	71 (0.44)	74 (0.23)	42 (0.23)	92 (0.22)	< 0.001
Acute renal failure	1 (0.006)	8 (0.025)	7 (0.038)	15 (0.037)	0.227
At least one complication, n (%)	757 (4.7)	1,197 (3.8)	808 (4.4)	1,686 (4.1)	< 0.001
Age ≤ 64 years	264 (4.0)	254 (2.9)	248 (3.6)	106 (3.0)	
65–79	384 (5.0)	716 (3.9)	467 (4.6)	1,114 (4.1)	
≥ 80	109 (6.0)	227 (5.0)	93 (6.7)	466 (4.9)	

of outcome might have occurred. Although we could not verify data for each patient, we presume the level of miscoding is low because DPC data are coded by physicians and subject to an audit. Data are limited as the DPC database does not record some important clinical data, such as the severity of the disease, levels of the arthrodesis, or type of implant used. Despite these limitations, the results presented here provide important national estimates of inpatient morbidity and mortality after orthopaedic surgery.

Table 3 Adjusted risk of adverse outcomes after surgery

	Inhospital death			Postoperative complications		
	OR	95% CI	p	OR	95% CI	p
Age						
≤ 64	Reference			Reference		
65–79	2.58	1.36 – 4.89	0.004	1.22	1.09 – 1.36	0.001
≥ 80	5.88	2.93 – 11.8	<0.001	1.51	1.31 – 1.75	< 0.001
Sex						
men	Reference			Reference		
women	0.60	0.39 – 0.92	0.018	0.88	0.82 – 0.95	0.001
Charlson comorbidity index						
0	Reference			Reference		
1	1.60	0.89 – 2.87	0.116	2.42	2.17 – 2.71	< 0.001
2	6.58	3.99 – 10.8	<0.001	3.42	2.92 – 4.01	< 0.001
≥ 3	16.50	10 – 27.2	<0.001	5.06	4.2 – 6.1	< 0.001
Surgical procedure						
Total knee arthroplasty	Reference			Reference		
Cervical laminoplasty	2.15	1.23 – 3.77	0.008	1.02	0.81 – 1.28	0.865
Lumbar decompression	1.38	0.79 – 2.4	0.253	0.87	0.72 – 1.04	0.117
Lumbar arthrodesis	2.23	1.21 – 4.06	0.009	1.07	0.92 – 1.24	0.397

OR odds ratio, *CI* confidence interval.